SCIENTIFIC REPORTS

OPEN

SUBJECT AREAS:
PHYSICAL SCIENCES
CHEMISTRY
CATALYSIS
PHOTOCATALYSIS

Received
22 July 2013

Accepted
30 August 2013

Published
17 September 2013

Correspondence and requests for materials should be addressed to J.S.L. (jlee1234@unist.ac.kr)

Single-crystalline, wormlike hematite photoanodes for efficient solar water splitting

Jae Young Kim[1], Ganesan Magesh[1], Duck Hyun Youn[1], Ji-Wook Jang[1], Jun Kubota[2], Kazunari Domen[2] & Jae Sung Lee[3]

[1]Department of Chemical Engineering, Pohang University of Science and Technology (POSTECH), San 31, Hyoja-dong, Pohang 790-784, Republic of Korea, [2]Department of Chemical System Engineering, The University of Tokyo, 7-3-1 Hongo, Bunkyo-ku, Tokyo 113-8656, Japan, [3]School of Energy and Chemical engineering, Ulsan National Institute of Science and Technology, 50 UNIST-gil, Ulsan 689-798, Republic of Korea.

A hematite photoanode showing a stable, record-breaking performance of 4.32 mA/cm^2 photoelectrochemical water oxidation current at 1.23 V vs. RHE under simulated 1-sun (100 mW/cm^2) irradiation is reported. This photocurrent corresponds to ca. 34% of the maximum theoretical limit expected for hematite with a band gap of 2.1 V. The photoanode produced stoichiometric hydrogen and oxygen gases in amounts close to the expected values from the photocurrent. The hematitle has a unique single-crystalline "wormlike" morphology produced by in-situ two-step annealing at 550°C and 800°C of β-FeOOH nanorods grown directly on a transparent conducting oxide glass via an all-solution method. In addition, it is modified by platinum doping to improve the charge transfer characteristics of hematite and an oxygen-evolving co-catalyst on the surface.

Hydrogen is considered a clean and storable energy carrier of the future if it could be produced from a renewable energy source via a CO_2-neutal and efficient route. Solar water splitting is such a renewable and sustainable energy production method because it can utilize the sun light, the most abundant energy source on earth, and water, the most abundant natural resource on earth. Water splitting can be carried out with coupled solar cell–water electrolysis systems, but efficiency loss between the two systems and high installation cost make them a less attractive option. As an alternative route, the direct photoelectrochemical (PEC) cell is potentially more economic because it combines the functions of a solar cell and an electrolyzer in a single device.

In a typical PEC cell, a light-absorbing semiconductor electrode and a metallic counter electrode are immersed in an aqueous electrolyte solution as shown in Fig. 1. When the photo-electrode is irradiated with photons that have an energy equal to or above the band gap of the semiconductor, electrons are photo-excited from the valence band of the semiconductor into its conduction band. The photoelectrons travel to the back contact and are transported via the electrical circuit to the counter electrode, where they reduce water to form hydrogen. The photo-generated holes in the valence band diffuse to the semiconductor-electrolyte interface, where they oxidize water to form oxygen. Since the pioneering demonstration of PEC water splitting by Fujishima and Honda[1], the storage of solar energy in the form of the hydrogen fuel has attracted worldwide attention[2–6].

The selection of the semiconductor electrodes is of paramount importance in PEC water splitting cells and the electrode materials have to satisfy a number of requirements. They should have a proper band gap energy (~2 eV) to cover water dissociation energy (1.23 eV) and strong visible light absorption, band edge positions enabling oxidation and reduction of water (0 and 1.23 V vs. RHE, respectively), chemical and electrochemical stability in water under illumination, fast transport of the photo-generated electrons and holes in the semiconductor, low over-potentials for the electrode reactions, and low cost[7–10].

Hematite (α-Fe_2O_3) satisfies many of these material requirements; a small band gap (~2.1 eV) that allows 15.3% of theoretical solar-to-hydrogen (STH) efficiency (or photocurrent generation of 12.6 mA/cm^2 at 1.23 V vs. RHE under 1-sun irradiation), excellent stability under alkaline conditions, low price, and environmentally benign characteristics[11–14]. Thus it has been a most popular and promising candidate of photoanode material for PEC solar water splitting over last two decades. However, hematite has a major and critical drawback, *i.e.* extremely poor electrical conducting property with a hole diffusion length of 2–4 nm[15,16]. Thus most of the hematite anodes have exhibited very low PEC performance because of the excessive charge recombination in the

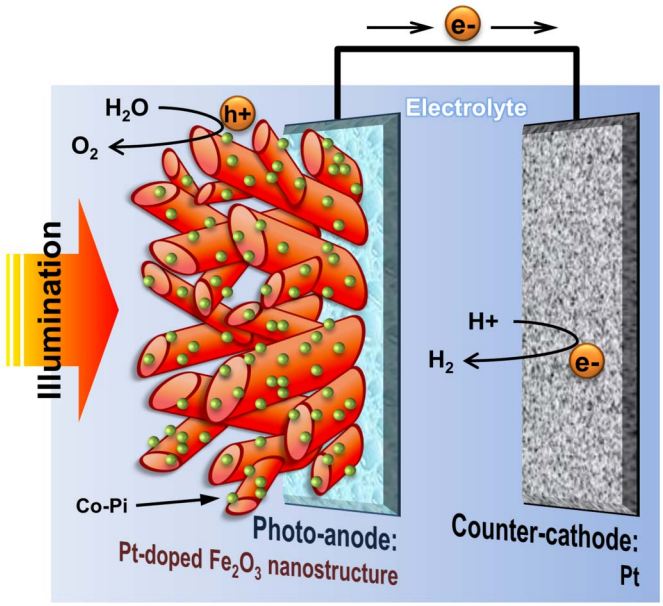

Figure 1 | Schematic diagram for a photoelectrochemical cell with the hematite thin film photoanode. The anode has Pt-doped, highly crystalline worm-like nanostructure modified with Co-Pi as an oxygen evolution co-catalyst on its surface. Charge recombination can be effectively suppressed with the help of the promoted charge separation at both the inside and outside of the photoanode by Pt-doped nanostructure and Co-Pi loading, respectively.

electrode. Hence, recent studies have focused on improving their charge transfer properties and encouraging results are being reported last few years. There are a number of approaches known to improve the electric properties of hematite. Doping is commonly employed to improve the electrical conducting property of hematite by increasing donor density[17–22]. Synthesis of nanostructures including one-dimensional (1-D) nanorods, nanowires, and nanotubes shortens the pathway that photoexcited electrons/holes have to travel[22–26]. Other successful approaches include making hematite-based composite photoanode with a good conducting material[27–30], forming a junction structure with another semiconducting material with a different band gap[31,32], or loading a co-catalyst on the semiconductor surface to facilitate oxygen evolution reaction (OER)[33–36]. Most of the previous works focused on a single specific aspect of these modifications, and thus the overall performance was not necessarily high.

In the present study, we report an α-Fe_2O_3 photoanode for PEC water splitting with a unique single-crystalline "wormlike" morphology produced by in-situ two-step annealing at 550°C and 800°C of 1-D β-FeOOH nanorods grown directly on a transparent conducting oxide (TCO) glass via an all-solution method[28,29]. In addition, we employed Pt-doping to improve the electrical conducting property of hematite and a co-catalyst (*e.g.* cobalt phosphate, Co-Pi) as a surface modification to help oxygen evolution reaction occur at a reduced over-potential. As a result, we obtained a wormlike hematite photoanode (schematically exhibited in Fig. 1) exhibiting the record-breaking PEC water oxidation activity (4.32 mA/cm^2 at 1.23 V vs. RHE under simulated 1-sun irradiation, 100 mW/cm^2). This photocurrent corresponds to ca. 34% of the maximum theoretical limit expected for hematite with a band gap of 2.1 V. This hematite photoanode was also very stable and produced stoichiometric hydrogen and oxygen gases (2 : 1) in amounts close to the expected values from the photocurrent.

Results

Fabrication of a single-crystalline, wormlike hematite photoanodes. As mentioned, hematite itself has a very poor electrical conducting property and thus charge carriers get trapped in the bulk of hematite and recombine to lower the efficiency. To alleviate this problem, we intended to fabricate hematite with the following characteristics; i) single-crystallinity with minimal charge trapping defects, and ii) highly non-isotropic morphology. For example, if 1-D nanorod of a high aspect ratio is formed, its lateral dimension matches the short hole diffusion length of hematite and electrons could flow though a direct pathway along the axial direction of the rods. Thus we adopted a modified version of the template-less thin film processing technique developed by Vayssieres et al.[37,38] to grow a highly anisotropic β-FeOOH akagenite film on F:SnO_2 (FTO)-coated glass from an aqueous $FeCl_3 \cdot 6H_2O$ solution in such conditions that the thermodynamic stabilization of the oxyhydroxide structure could be secured. This β-FeOOH nanostructure on FTO was then converted to α-Fe_2O_3 by thermal treatment.

Fig. 2A shows SEM and TEM images of β-FeOOH nanorods of 30 nm in diameter and 500 nm in length (aspect ratio 1 : 17) roughly perpendicular to the FTO glass substrate. The *yellow* β-FeOOH thin film were thoroughly rinsed with water and subsequently annealed in air at 550°C for one hour to allow a complete crystal phase transition to the *orange-red* hematite (α-Fe_2O_3) as confirmed by XRD (reference pattern number: 01-085-0599). As shown in Fig. 2B, the nanorod morphology was conserved with little change in the anisotropic dimensions. This is the usual condition that most of the hematite films were annealed before PEC water splitting tests in the literature because the higher temperature treatment would degrade the conductivity of FTO. However, this hematite nanorod film exhibited a poor PEC water splitting performance. Hence, we increased the annealing temperature further to 800°C considering the report that this extremely high temperature annealing enhanced the PEC activity of hematite[39,40]. Of course, excessive annealing increases the resistance of FTO as shown in Table S1, which offsets favorable effects of increasing crystallinity of hematite. We found that 20 min was the optimum annealing time that gave the highest photocurrent. In Fig. 2C, the nanorod morphology changed totally to a worm-like structure with bigger feature sizes (50 nm × 500 nm) after 800°C annealing, while still maintaining hematite crystal structure. When the TEM images of Fig. 2B and C were examined on the same scale, the hematite thin film annealed at 550°C showed crystallized areas (inside the dotted lines) that were small and separated from each other indicating polycrystallinity (multiple particles), while the film annealed at 800°C showed a single crystalline character without any grain boundaries. The lattice fringes in the HRTEM image of the single crystal (Fig. 2B) are separated by ~2.5 Å, which agreed well with the {110} lattice spacing of hematite.

In Fig. S1, cross-sectional TEM images of the hematite thin films are presented. The thickness of the films was almost the same (~500 nm) before and after annealing at 550 or 800°C, but the morphology changed as the annealing temperature increased. Bundles of nanorods are close-packed in unannealed and 550°C-annealed films. On the other hand, the 800°C-annealed film show enlarged feature size and more blank spaces within the thin film (white area in Fig. S1C) are developed. In XRD analysis of the hematite films shown in Fig. S2, the peak corresponding to (110) of α-Fe_2O_3 is dominant possibly due to preferential orientation of the hematite nanostructure. Conductivities in the (001) basal planes (*e.g.* in the [110] direction) have been measured up to 4 orders of magnitude higher than in the perpendicular direction[41–43]. Thus the hematite thin film prepared by the current method is dominantly developed with the highly conductive (001) basal planes perpendicular to the substrate. The XRD pattern of 800°C-annealed hematite in Fig. S3 shows similar feature for hematite but sharper diffraction peaks from FTO.

The single-crystalline wormlike hematite was then modified by impurity doping. Among many possible effects of doping, relevant to this work is enhancement in the electrical conductivity through

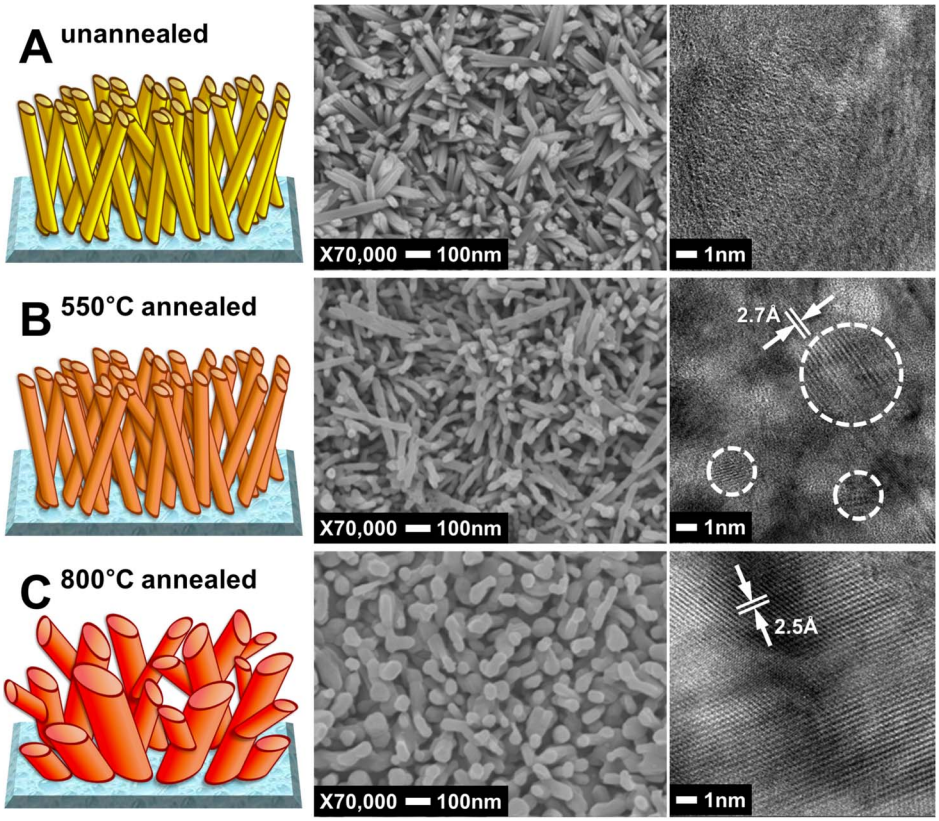

Figure 2 | **SEM and TEM images of the hematite thin films; unannealed (A), annealed at 550°C (B), and annealed at 800°C (C).**

modified charge-carrier properties *i.e.* mobility, carrier concentration or efficient separation of photogenerated charge carriers through a built-in electrical field near the solid-liquid interface. Among many known dopants for hematite, we employed Pt inspired by the work of Hu *et al.*[17], which reported a dramatically improved PEC performance of thin film photoanodes of nanocrystalline Pt-doped iron oxide prepared by an electrodeposition method. We just added the Pt precursor (chloroplatinic acid) into the preparation solution of the β-FeOOH thin film and treated the film by the two-step annealing under the same conditions for preparation of the un-doped hematite film. According to SEM-EDS mapping in Fig. S4, Pt is uniformly distributed over the hematite thin film. The Pt/Fe ratio calculated from the SEM-EDS results was 3.33%, although the initally added amount was 5% selected by a prelmnary optimization process. The films of Pt-doped hematite had the same worm-like structure as that of undoped films, although its feature and bulk pore size was slightly bigger than those of the undoped film.

Another modification of hematite film is the introduction of a co-catalyst for oxygen evolution reaction (OER). We tried several known OER catalysts including cobalt phosphate (Co-Pi), IrO_2 nanoparticles, and RuO_2, and found that Co-Pi gave the best results. The Co-Pi has been extensively studied as a water oxidation co-catalyst for many semiconductor photocatalyst systems[16,33–36,44–46]. This oxygen evolving catalyst containing cobalt oxide and hydroxide species works well in a phosphate buffer solution. Thus, Co-Pi was deposited on Pt-doped hematite electrode by photo-assisted electrodeposition at an optimized condition of 0.1 V vs. Ag/AgCl for 30 sec to form a thin catalyst layer.

PEC water splitting activity of wormlike hematite photoanodes. The photoelectrochemical water splitting activity was studied first for small 1 cm × 1 cm of the hematite photoanodes in a three-electrode cell as working electrodes to observe their PEC water oxidation response under 1 sun (100 mW/cm^2) and AM 1.5 G simulated solar light irradiation. A platinum mesh electrode, Ag/AgCl electrode, and 1 M NaOH were also employed in the cell as counter electrode, reference electrode, and electrolyte, respectively. Fig. 3A shows photocurrent response under chopped light to applied anodic potentials (*I-V* curve) for the prepared hematite photoanodes; bare Fe_2O_3, Pt-doped Fe_2O_3 (Pt:Fe_2O_3), and Pt-doped Fe_2O_3 modified with Co-Pi (Pt:Fe_2O_3/Co-Pi). In the dark, the *I-V* response for all the samples is similar and shows no currents below 1.7 V vs. RHE. The photocurrent observed under illumination is a direct measure of the rate of water splitting and reflects the number of charge carriers produced from the incident light and their subsequent participation in water oxidation reaction on the photoanode and hydrogen ion reduction on the counter electrode. The performance of the photoanode is commonly compared at 1.23 V vs. RHE, the theoretical water oxidation potential. The bare hematite marks a photocurrent of 1.26 mA/cm^2, which represents one of the highest photocurrents reported for bare hematite photoanodes under this standard condition[47–51]. This good performance may originate from two sources; i) the highly anisotropic morphology derived from β-FeOOH precursor of 1-D nanorod structure, and ii) high crystallinity and interconnectivity of hematite particles due to the annealing at 800°C. These are attributes of efficient photoelectrode materials facilitating charge transfer and minimizing charge recombination. Upon Pt doping (5% Pt:Fe_2O_3), the photocurrent increases by 74% to 2.19 mA/cm^2. This improvement by Pt-doping is qualitatively consistent with the report of Hu *et al.*[17], although our absolute current value is much higher than theirs because our bare hematite performs better as discussed above. Finally, when Pt:Fe_2O_3 is modified with the Co-Pi co-catalyst (Pt:Fe_2O_3/Co-Pi), the generated photocurrent increases by additional 170% to 4.32 mA/cm^2, which is the highest stable PEC water oxidation current for hematite photoanode ever reported.

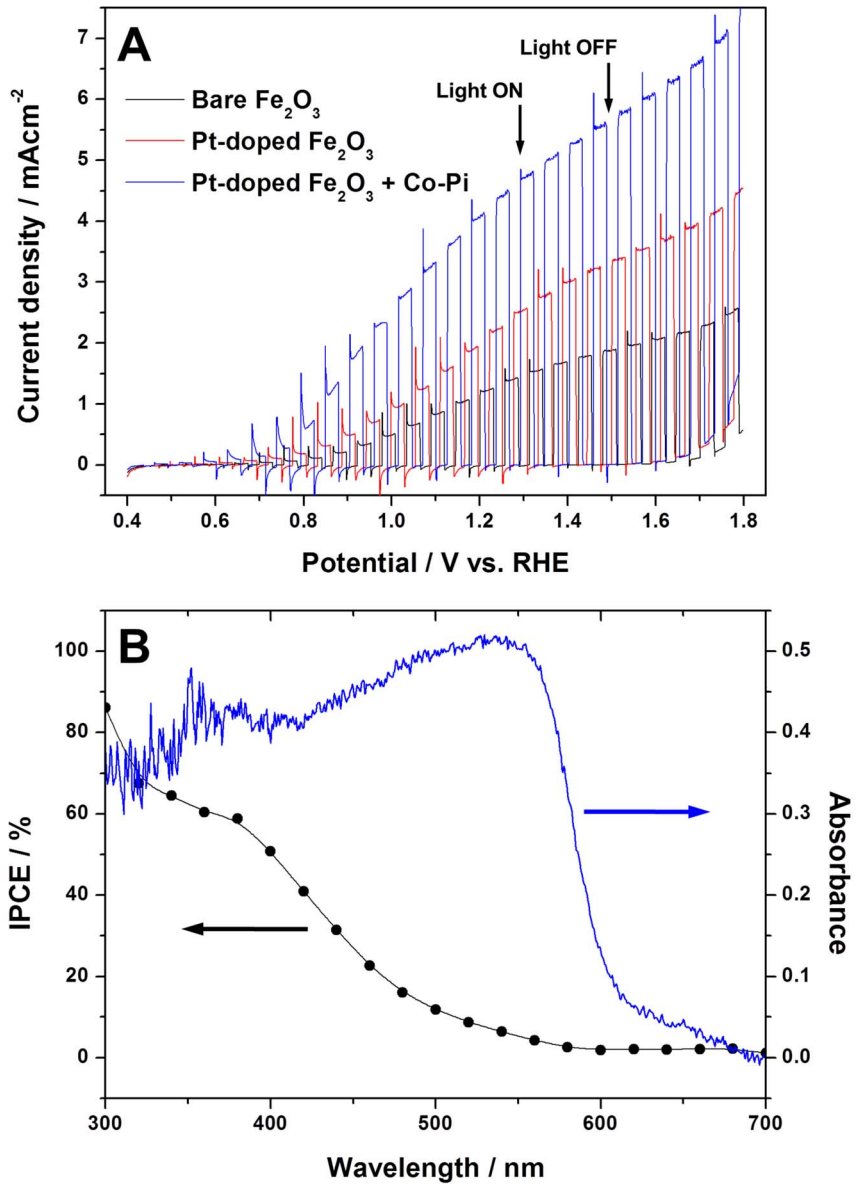

Figure 3 | (A) Photocurrent-potential (*I-V*) curves for PEC water oxidation reaction with the hematite photoanodes; (B) IPCE and UV-Vis absorption spectrum of the Pt-doped hematite photoanode modified with Co-Pi.

In Fig. 3B, the incident photon-to-current efficiency (IPCE) as a function of wavelength for Pt:Fe_2O_3/Co-Pi thin film is presented together with its UV-Vis absorption spectrum. The absorbance increased sharply from 600 nm towards low wavelengths, which is consistent with band gap of hematite (~2.1 eV) and follows roughly the observed IPCE behavior between 400 and 600 nm. It indicates that absorbed photons of different energies have been successfully converted to photocurrents. In particular, the IPCE values at short wavelength region (<400 nm) are very high, 60–80%. These are also unprecedented IPCE values for hematite photoanodes that typically show IPCE values even below 10%[49]. It indicates that our Pt:Fe_2O_3/Co-Pi converts the incident high energy photons to current exremely well. But IPCE decreased much more rapidly over 400–600 nm region than absorption spectrum. Thus, IPCE at long wavelengths near band gap energies is much lower, which is a common characteristic of hematite photoelectrode. This is because absorption in this region is due to the indirect d → d transition of Fe^{3+}, and electron-hole pair generated by this transition is localized in Fe^{3+} and are not used effectively to generate water oxidation photocurrent.

In order to confirm that the photocurrents observed in the three-electrode PEC cell (Fig. 3A) was really due to PEC water splitting, we constructed a closed circulation PEC system shown in Fig. S5, where the photocurrents and evolved hydrogen/oxygen could be measured simultaneously. At the same time, we enlarge the size of the Pt:Fe_2O_3/Co-Pi photoanode to 2 cm × 2 cm to examine the effect of scale-up and for better analysis of gaseous products. A blank test demonstrated that there was no hydrogen/oxygen evolution without irradiation or a photoanode. In Fig. 4, both hydrogen and oxygen gases are evolved linearly with time and the ratio of evolved hydrogen to oxygen was close to 2 (Table S2) as expected from the stoichiometry of the water splitting reaction.

$$\text{At anode}: \quad 2H_2O(l) + h\nu \rightarrow O_2(g) + 4H^+ + 4e^- \qquad (1)$$

$$\text{At cathode}: \quad 2H^+ + 2e^- \rightarrow H_2(g) \qquad (2)$$

The H_2/O_2 gas evolution was accompanied by a stable current density of 4.0 mA/cm^2 as presented by chronoamperometry in Fig. S6. Thus, there is no significant decrease of photocurrent density

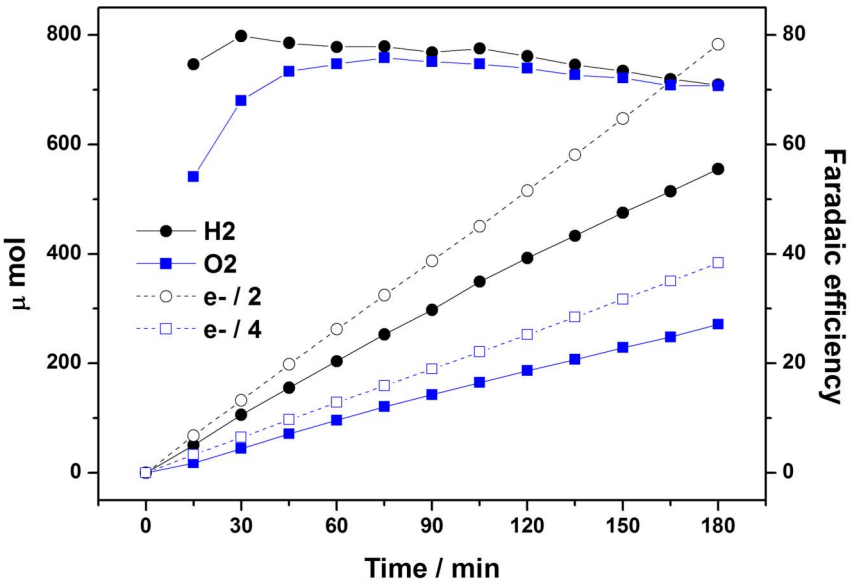

Figure 4 | Evolution of hydrogen/oxygen from the Pt-doped hematite photoanode modified with Co-Pi is compared with the evolution of H_2 ($e^-/2$) and O_2 ($e^-/4$) expected from current generation. Ratios between these two sets of gas evolution (faradaic efficiency) were also displayed in the right y-axis. Photocurrent-time curve recorded with this measurement is supplied in Fig. S6.

when the Pt:Fe_2O_3/Co-Pi photoanode was enlarged from 1 × 1 cm^2 (4.32 mA/cm^2) to 2 × 2 cm^2 (~4.0 mA/cm^2). Fig. 4 also shows theoretical gas evolution rates calculated from the generated current. According to equations 1 and 2, four and two electrons are necessary to produce oxygen and hydrogen respectively for solar water splitting in a PEC cell. The ratio between the measured and predicted gas evolution rates gives faradaic efficiency of 70–80% during the whole measurements (Table S2). Thus, most of the photogenerated charges were consumed for water splitting and hydrogen/oxygen production in the current system. When we applied another bias potential of 1.5 V vs. RHE instead of 1.23 V vs. RHE to the system, the faradaic efficiency was almost 100% during the measurement (not shown), indicating that efficiency loss is reduced at high applied potentials. Hence it has been demonstrated that our solution-based synthesis method could be applied to fabrication of large scale hematite photoanodes.

Our wormlike Pt:Fe_2O_3/Co-Pi photoanode shows a record breaking high activity and stability for PEC water splitting under simulated solar light. To show where the performance of our photoanodes stands, we plot in Fig. 5 our data together with data of Sivula *et al.*[11], which summarize a history of performance improvement of PEC water oxidation with hematite photoanodes presented in terms of current density generated under the standard condition (1 sun and 1.23 V vs. RHE). For past two decades, the photocurrent has gradually increased with the development of various preparation (ultrasonic spray pyrolysis, atmospheric pressure chemical vapor deposition (APCVD)) and modification (Si-doping, Co-Pi deposition) techniques for hematite photoanodes. Our unmodified wormlike hematite already shows comparable activity to that of Si-doped hematite prepared by ultrasonic spray pyrolysis. As mentioned, this good activity is due to the formation of the highly anisotropic morphology and single-crystallinity derived from our unique synthesis method and two-step annealing treatment. Two modifications, *i.e.* Pt-doping and OER co-catalyst produced the Pt:Fe_2O_3/Co-Pi photoanode that easily broke the world performance record. This photocurrent of 4.32 mA/cm^2 at 1.23 V vs. RHE under 1-sun irradiation corresponds to ca. 34% of the maximum theoretical limit expected for hematite with a band gap of 2.1 V (12.6 mA/cm^2). Many PEC water splitting projects around the world expect eventually *ca.* 50% or 6–7 mA/cm^2 from hematite-based photoanodes. The performance also marks the best record among all stable oxide semiconductor-based photoanodes. Thus our result could be a meaningful milestone leading to the final goal, and it also has demonstrated that the carefully designed fabrication and modification strategies are effective for extracting the best performance out of the known electrode materials.

It should be noted that the photocurrents in Fig. 3A were measured at 1.23 V (vs. RHE) of applied voltage. If we take out the contribution of this external energy supply, the net solar energy-to-current efficiency is only ca. 0.6% at most as shown in Fig. S7. In practice, the PEC system will operate in a tandem mode where a photovoltaic cell is placed behind the water photolytic cell to provide the bias voltage using transmitted sunlight through the transparent photoelectrode. Hence, we need to develop a low price photovotaic cell that could supply >1 V by using the transmitted sunlight only in oder to make the tandem PEC cell practical.

Electrochemical study of photoanodes. To show that our modifications indeed led to the improved charge transfer characteristics of the hematite photoanode, we conducted Mott-Schottky analysis and electrochemical impedance spectroscopy (EIS). Donor density and flat band potential of the hematite photoanodes were estimated from the results of Mott-Schottky analysis[52]. From the slope of the Mott-Schottky plot in Fig. S8, the determined donor density was 3.27 × 10^{17} cm^{-3}, 2.77 × 10^{18} cm^{-3}, and 3.91 × 10^{18} cm^{-3} for bare Fe_2O_3, Pt:Fe_2O_3, and Pt:Fe_2O_3/Co-Pi, respectively. Obviously, Pt-doping was effective to improve the electrical conducting property of hematite by increasing its donor density. The flat band potential shifted slightly to positive values in the Pt-doped hematite photoanodes. This result is possibly due to additional donor level formed by Pt-doping.

In Fig. 6A, Nyquist plots of the hematite photoanodes obtained from potentiostatic EIS are presensented[52–55]. The symbols in this figure represent experimental data and the solid lines represent results of fitting the data to an equivalent circuit model shown in Fig. 6B. All the hematite photoanodes were best fitted to a 2-RC-circuit model which contains one resistor and two RC circuits (sub-circuit with a resistor R and a capacitor C in parallel) in series. Two RC circuits can be assigned to Fe_2O_3||electrolyte and bulk Fe_2O_3, two major interfaces within photoanodes dominantly developing

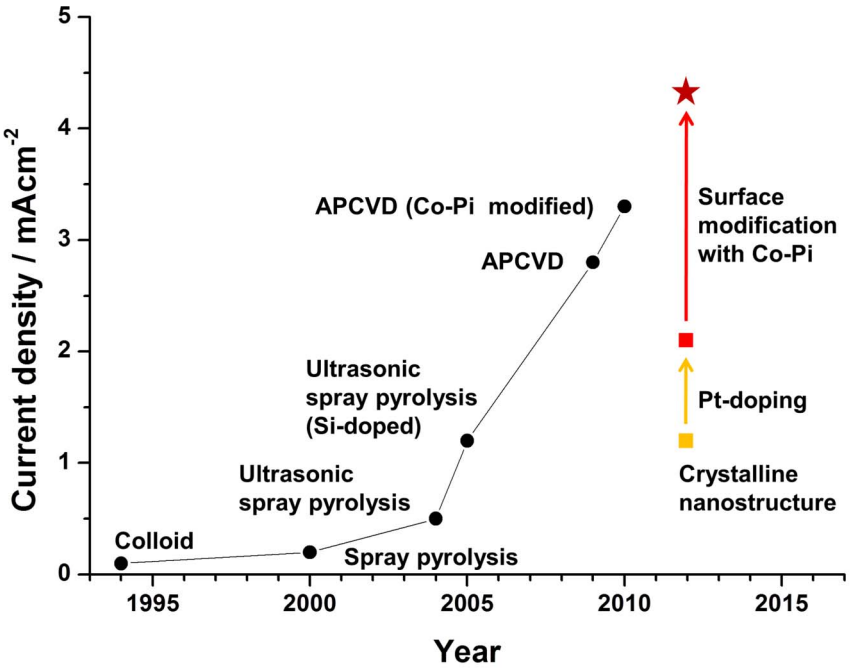

Figure 5 | Historical improvement in the performance of hematite photoanodes are presented in terms of photoelectrochemical water oxidation current density generated under standard condition (1 sun and 1.23 V vs. RHE)[11].

impedance elements as assigned in the previdous studies[27,28]. The most difficult reaction occuring at photoanode, *i.e.* water oxidation, takes place at Fe_2O_3||electrolyte, hence the biggest charge transfer resistance and double layer capacitance are generally observed here. Naturally the remaining RC circuit is assigned to bulk Fe_2O_3. The most interesting of the fitting result is that Pt-doping remarkably affects the charge trransfer characteristics of the entire hematite photoanodes including Fe_2O_3||electrolyte and bulk Fe_2O_3, whereas Co-Pi modification affects only the subcircuit corresponding to Fe_2O_3||electrolyte. For the Pt-doped hematite photoanodes, all charge transfer resistances decreased and capacitances increased, implying that Pt-doping promoted charge separation at any position of the bulk photoanode and finally enhanced its PEC water splitting ability. On the other hand, Co-Pi modification reduced the charge transfer resistance and increased the capacitance mainly at Fe_2O_3||electrolyte, *i.e.* the surface of the photoanode at which water oxidation reaction takes place. Therefore we can conclude that Co-Pi loading promotes the charge separation and water oxidation reaction on the surface of hematite photoanode.

Discussion

We prepared single-crystalline wormlike hematite film on FTO by first forming 1-D β-FeOOH nanorods as the precursor and then converting them to α-Fe_2O_3 by two-step annealing treatment. In addition, we adopted platinum doping to improve the charge transfer characteristics in the bulk of the hematite, and an oxygen evolution cocatalyst (Co-Pi) to modify the surface properties. As a result, the hematite photoanode showed a record-breaking performance of 4.32 mA/cm^2 photoelectrochemical water oxidation current at 1.23 V vs. RHE under simulated 1-sun (100 mW/cm^2) irradiation. This corresponds to ca. 34% of the maximum theoretical limit expected for hematite with a band gap of 2.1 V. The photoanode kept its high and stable activity for production of stoichiometric hydrogen and oxygen evolution in a large size electrode, demonstrating its durability and scalability. Mott-Schottky analysis and EIS demonstrated the effectiveness of Pt-doping and Co-Pi modification to improve the charge transfer properties of hematite. Our result could be a meaningful milestone leading to the final goal (6–7 mA/cm^2 expected from hematite anodes) and it also has demonstrated that the carefully designed fabrication and modification strategies are effective for extracting the best performance out of the known electrode materials.

Methods

Preparation of the hematite thin film photoanodes. The hematite photoanodes were prepared via a simple solution-based method[37] and two-step annealing. First, a starting material is grown on substrate (F:SnO_2 coated glass) at 100°C in aqueous solution containing Fe precursor (0.15 M $FeCl_3 \cdot 6H_2O$) and Pt precursor (chloroplatinic acid). Thickness of thin film can be controlled by varying the aging time. In the present study, the reactor containing the previous solution was kept in an oven for 6 h and the resultant thin film had the thickness of ~500 nm (Fig. S1), which showed the best performance in the current synthesis method. After the preparation, the substrate coated with yellow thin film was annealed via two-step annealing, the initial annealing at 550°C for 1 h followed by 20 min-short annealing at 800°C. This yellow thin film turns to orange and orange-red after 550 and 800°C annealing, respectively. For deposition of Co-Pi on the surface of the Pt-doped hematite thin film, photo-assisted electrodeposition (PED) was adopted[26]. The 1 sun-simulated solar light was used as light source for PED and 0.1 M potassium phosphate buffer solution at pH 7 was used as an electrolyte. Applied bias potential 0.0–0.3 V vs. Ag/AgCl and deposition time 5–180 s were tried to find the best condition for high activity of the hematite photoanodes, *i.e.* 0.1 V vs. Ag/AgCl and 10 s were chosen. After PED, the Pt-doped hematite photoanode modified with Co-Pi was also washed with distilled water.

Catalyst characterization and photoelectrochemical studies. In order to characterize the hematite thin films, x-ray diffraction analysis (PW3040/60 X'pert PRO, PANalytical with Cu Kα (λ = 1.54056 Å) radiation), high resolution scanning electron microscopy (JSM-7401F, JEOL), and high resolution transmission electron microscopy (JEM-2200FS, JEOL with Cs-corrector in the National Center for Nanomaterials Technology, Korea were used.

The photoanode was put in a three electrode cell as a working electrode to observe its PEC water oxidation response. A platinum mesh electrode, Ag/AgCl electrode, and 1 M sodium hydroxide were also employed in the cell as a counter electrode, reference electrode, and electrolyte, respectively. Photocurrent-potential curves, photocurrent-time curves and electrochemical impedance spectra were recorded under simulated solar light generated by a solar simulator (91160, Oriel) with an air mass 1.5 G filter. Light intensity of the solar simulator was calibrated to 1 sun (100 mW/cm^2) using a reference cell certified by the National Renewable Energy Laboratories, U.S. When incident photon conversion efficiency (IPCE) was recorded, the cell was irradiated by a 300 W xenon lamp (66905, Oriel Instruments) coupled with a monochromator (74004, Oriel Conerstone). A 299 nm cut off filter was also placed at the exit of the output to prevent λ/2 radiation originated by Bragg diffraction at the grating. Measurement of stable constant photocurrent and IPCE were carried out at 1.23 V vs. RHE. During the measurement of stable constant photocurrent, evolved hydrogen/oxygen amount was recorded by gas chromatography. We used the closed circulation system (Fig. S5) for this experiment and Ar was used as a carrier gas. Electrochemical

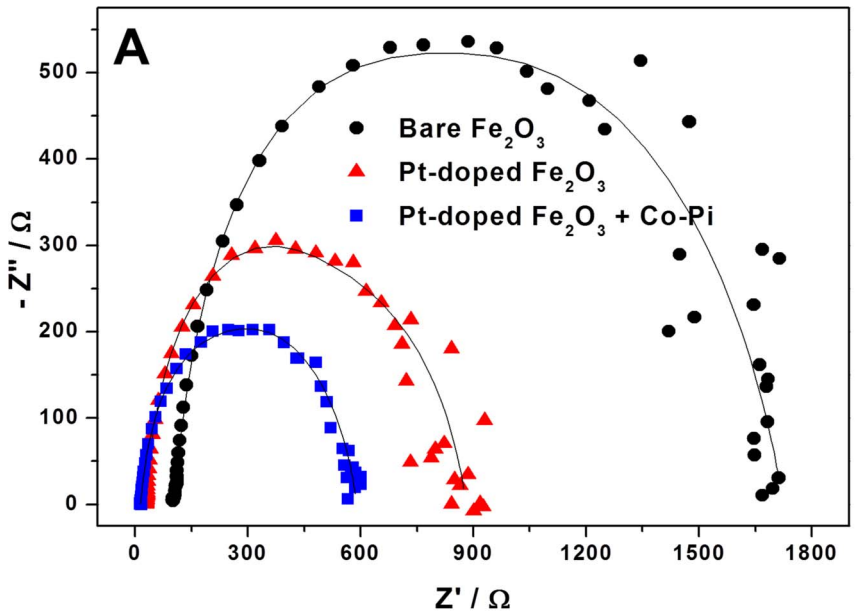

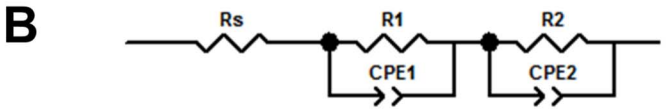

(R / Ω) (CPE / F)	Rs	R1 CPE1	R2 CPE2
Bare Fe_2O_3	109	725 5.84×10^{-6}	1176 3.36×10^{-5}
Pt-doped Fe_2O_3	31.2	284 1.23×10^{-5}	601 1.01×10^{-4}
Pt-doped Fe_2O_3 + Co-Pi	14.8	290 1.95×10^{-5}	349 2.18×10^{-4}

Figure 6 | Nyquist plots of the hematite photoanodes; (B) the equivalent circuit model used for fitting the experimental data in A and the fitting results.

impedance spectra were recorded at DC potential of 1.23 V vs. RHE and an AC potential frequency range of 100000–0.1 Hz with an amplitude of 10 mV. A potentiostat (IviumStat, Ivium Technologies) was used for applying bias potential to the cell and a software (ZView, Scribner Associates) was used for fitting the experimental EIS data to the equivalent circuit model. Mott-Schottky analysis was carried out at a DC potential range of 0.4–1.4 vs. RHE with an AC potential frequency 10 kHz under dark condition. The amplitude of AC potential was 10 mV.

1. Fujishima, A. & Honda, K. Electrochemical photolysis of water at a semiconductor electrode. *Nature* **238**, 37–38 (1972).
2. Grätzel, M. Photoelectrochemical cells. *Nature* **414**, 338–344 (2001).
3. Tachibana, Y., Vayssieres, L. & Durrant, J. R. Artificial photosynthesis for solar water-splitting. *Nat. Photonics* **6**, 511–518 (2012).
4. Walter, M. G. *et al.* Solar water splitting cells. *Chem. Rev.* **110**, 6446–6473 (2010).
5. Bard, A. J. & Fox, M. A. Artificial photosynthesis: Solar splitting of water to hydrogen and oxygen. *Acc. Chem. Res.* **28**, 141–145 (1995).
6. Bak, T., Nowotny, J., Rekas, M. & Sorrell, C. C. Photo-electrochemical hydrogen generation from water using solar energy. Materials-related aspects. *Int. J. Hydrogen Energy* **27**, 991–1022 (2002).
7. van de Krol, R., Liang, Y. & Schoonman, J. Solar hydrogen production with nanostructured metal oxides. *J. Mater. Chem.* **18**, 2311–2320 (2008).
8. Yin, W.-J. *et al.* Band structure engineering of semiconductors for enhanced photoelectrochemical water splitting: The case of TiO_2. *Phys. Rev. B* **82**, 045106–045111 (2010).
9. Holladay, J. D., Hu, J., King, D. L. & Wang, Y. An everview of hydrogen production technologies. *Catal. Today* **139**, 244–260 (2007).
10. Rauh, R. D., Buzby, J. M., Reise, T. F. & Alkaitis, S. A. Design and evaluation of new oxide photoanodes for the photoelectrolysis of water with solar energy. *J. Phys. Chem.* **83**, 2221–2226 (1979).
11. Sivula, K., Le Formal, F. & Grätzel, M. Solar water splitting: progress using hematite (α-Fe_2O_3) photoelectrodes. *ChemSusChem* **4**, 432–449 (2011).
12. Itoh, K. & Bockris, J. O'M. Thin film photoelectrochemistry: iron oxide. *J. Electrochem. Soc.* **131**, 1266–1271 (1984).
13. Cai, S., Zhang, J., Lu, T., Lin, Y. & Yin, Q. Intermitent light-ac electricity conversion on iron oxide/electrolyte solution/platinum photoelectrochemical cell. *Electrochim. Acta* **37**, 1101–1103 (1992).
14. Beermann, N., Vayssieres, L., Lindquist, S.-E. & Hagfeldt, A. Photoelectrochemical studies of oriented nanorod thin films of hematite. *J. Electrochem. Soc.* **147**, 2456–2461 (2000).
15. Kennedy, J. H. & Frese, K. W. Flatband potentials and donor densities of polycrystalline α-Fe_2O_3 determined from Mott-Schottky plots. *J. Electrochem. Soc.* **125**, 709–714 (1978).
16. Tilley, S. D., Cornuz, M., Sivula, K. & Grätzel, M. Light-induced water splitting with hematite: Improved nanostructure and iridium oxide catalysis. *Angew. Chem. Int. Ed.* **49**, 6405–6408 (2010).
17. Hu, Y.-S. *et al.* Pt-doped α-Fe_2O_3 thin films active for photoelectrochemical water splitting. *Chem. Mater.* **20**, 3803–3805 (2008).
18. Sartoretti, C. J. *et al.* Photoelectrochemical oxidation of water at transparent ferric oxide film electrodes. *J. Phys. Chem. B* **109**, 13685–13692 (2005).
19. Cesar, I., Kay, A., Gonzalez Martinez, J. A. & Grätzel, M. Translucent thin film Fe_2O_3 photoanodes for efficient water splitting by sunlight: n. anostructure-directing effect of Si-doping. *J. Am. Chem. Soc.* **128**, 4582–4583 (2006).
20. Choi, J., Park, H. & Hoffmann, M. R. Combinatorial doping of TiO_2 with platinum (Pt), chromium (Cr), vanadium (V), and nickel (Ni) to achieve enhanced photocatalytic activity with visible light irradiation. *J. Mater. Res.* **25**, 149–158 (2010).
21. Jo, W. J. *et al.* Phosphate doping into monoclinic $BiVO_4$ for enhanced photoelectrochemical water oxidation activity. *Angew. Chem. Int. Ed.* **51**, 3147–3151 (2012).

22. Mao, A., Park, J.-G., Han, G. Y. & Park, J. H. Controlled growth of vertically oriented hematite/Pt composite nanorod arrays: use for photoelectrochemical water splitting. *Nanotechnology* **22**, 175703 (2011).
23. Kim, H. G. *et al.* Engineered nanorod perovskite film photocatalysts to harvest visible light. *Adv. Mater.* **23**, 2088–2092 (2011).
24. Jun, H. *et al.* Photoelectrochemical water splitting over ordered honeycomb hematite electrodes stabilized by alumina shielding. *Energy Environ. Sci.* **5**, 6375–6382 (2012).
25. Prakasam, H. E., Varghese, O. K., Paulose, M., Mor, G. K. & Grimes, C. A. Synthesis and photoelectrochemical properties of nanoporous iron (III) oxide by potentiostatic anodization. *Nanotechnology* **17**, 4285–4291 (2006).
26. Borse, P. H., Jun, H., Choi, S. H., Hong, S. J. & Lee, J. S. Phase and photoelectrochemical behavior of solution-processed Fe_2O_3 nanocrystals for oxidation of water under solar light. *Appl. Phys. Lett.* **93**, 173103 (2008).
27. Kim, J. Y., Jun, H., Hong, S. J., Kim, H. G. & Lee, J. S. Charge transfer in iron oxide photoanode modified with carbon nanotubes for photoelectrochemical water oxidation: an electrochemical impedance study. *Int. J. Hydrogen Energy* **36**, 9462–9468 (2011).
28. Kim, J. Y. *et al.* Graphene-carbon nanotube composite as effective conducting scaffold to enhance the photoelectrochemical water oxidation activity of a hematite film. *RSC Advances* **2**, 9415–9422 (2012).
29. Ng, Y. H., Iwase, A., Kudo, A. & Amal, R. Reducing graphene oxide on a visible-light $BiVO_4$ photocatalyst for an enhanced photoelectrochemical water splitting. *J. Phys. Chem. Lett.* **1**, 2607–2612 (2010).
30. Ng, Y. H., Lightcap, I. V., Goodwin, K., Matsumura, M. & Kamat, P. V. *J. Phys. Chem. Lett.* **1**, 2222–2227 (2010).
31. Hong, S. J., Lee, S., Jang, J. S. & Lee, J. S. Heterojunction $BiVO_4/WO_3$ electrodes for enhance photoactivity of water oxidation. *Energy Environ. Sci.* **4**, 1781–1787 (2011).
32. Sivula, K., Le Formal, F. & Grätzel, M. WO_3-Fe_2O_3 photoanodes for water splitting: a host scaffold, guest absorber approach. *Chem. Mater.* **21**, 2862–2867 (2009).
33. Kanan, M. W., Surendranath, Y. & Nocera, D. G. Cobalt-phosphate oxygen-evolving compound. *Chem. Soc. Rev.* **38**, 109–114 (2009).
34. Kanan, M. W. & Nocera, D. G. In situ formation of an oxygen-evolving catalyst in neutral water containing phosphate and Co^{2+}. *Science* **321**, 1072–1076 (2008).
35. Zhong, D. K., Cornuz, M., Sivula, K., Grätzel, M. & Gamelin, D. R. Photo-assisted electrodepostion of cobalt-phosphate (Co-Pi) catalyst on hematite photoanodes for solar water oxidation. *Energy Environ. Sci.* **4**, 1759–1764 (2011).
36. Kanan, M. W. *et al.* Structure and valency of a cobalt-phosphate water oxidation catalyst determined by in situ x-ray spectroscopy. *J. Am. Chem. Soc.* **132**, 13692–13701 (2010).
37. Vayssieres, L., Beermann, N., Lindquist, S.-E. & Hagfeldt, A. Controlled aqueous chemical growth of oriented three-dimensional crystalline nanorod arrays: application to iron (III) oxides. *Chem. Mater.* **13**, 233–235 (2001).
38. Vayssieres, L., Keis, K., Hagfeldt, A. & Lindquist, S.-E. Three-dimensional array of highly oriented crystalline ZnO microtubes. *Chem. Mater.* **13**, 4395–4398 (2001).
39. Sivula, K. *et al.* Photoelectrochemical water splitting with mesoporous hematite prepared by a solution-based colloidal approach. *J. Am. Chem. Soc.* **132**, 7436–7444 (2010).
40. Brillet, J., Grätzel, M. & Sivula, K. Decoupling feature size and functionality in solution-processed, porous hematite electrodes for solar water splitting. *Nano Lett.* **10**, 4155–4160 (2010).
41. Cornuz, M., Gratzel, M. & Sivula, K. Preferential orientation in hematite films for solar hydrogen production via water splitting. *Chem. Vap. Deposition* **16**, 291–295 (2010).
42. Nakau, T. Electrical conductivity of α-Fe_2O_3. *J. Phys. Soc. Jpn.* **15**, 727–727 (1960).
43. Benjelloun, D. *et al.* Anisotropy of electrical properties of iron oxide. *Mater. Chem. Phys.* **10**, 503–518 (1984).
44. Liang, Y. *et al.* Co_3O_4 nanocrystals on graphene as a synergistic catalyst for oxygen reduction reaction. *Nat. Mater.* **10**, 780–786 (2011).
45. Dincă, M., Surendradath, Y. & Nocera, D. G. Nickel-borate oxygen-evolving catalyst that functions under benign conditions. *Proc. Natl. Acad. Sci.* **107**, 10337–10341 (2010).
46. Gamelin, D. R. Catalyst or spectator? *Nat. Chem.* **4**, 965–967 (2012).
47. Ling, Y., Wang, G., Wheeler, D. A., Zhang, J. Z. & Li, Y. Sn-doped hematite nanostructures for photoelectrochemical water splitting. *Nano Lett.* **11**, 2119–2125 (2011).
48. Takahashi, H. *et al.* Enhancement in the performance of ultrathin hematite photoanode for water splitting by an oxide underlayer. *Adv. Mater.* **24**, 2699–2702 (2012).
49. Li, Z., Luo, W., Zhang, M., Feng, J. & Zou, Z. Photoelectrochemical cells for solar hydrogen production: Current state of promising photoelectrodes, methods to improve their properties, and outlook. *Energy Environ. Sci.* **6**, 347–370 (2013).
50. Franking, R. *et al.* Facile post-growth doping of nanostructured hematite photoanodes for enhanced photoelectrochemical water oxidation. *Energy Environ. Sci.* **6**, 500–512 (2013).
51. Zandi, O., Klahr, B. M. & Hamann, T. W. Highly photoactive Ti-doped a-Fe_2O_3 thin film electrodes: Resurrection of the dead layer. *Energy Environ. Sci.* **6**, 634–642 (2013).
52. Zhang, W.-D., Jiang, J.-C. & Ye, J.-S. Photoelectrochemical study on charge transfer properties of ZnO nanowires promoted by carbon nanotubes. *J. Phys. Chem. C* **113**, 16247–16253 (2009).
53. Xie, Y., Zhou, L. & Lu, J. Photoelectrochemical behavior of titania nanotube array grown on nanocrystalline titanium. *J. Mater. Sci.* **44**, 2907–2915 (2009).
54. Tahir, A. A., Upul Wijazayantha, K. G., Saremi-Yarahmadi, S., Mazhar, M. & Mckee, V. Nanostructured α-Fe_2O_3 thin films for photoelectrochemical hydrogen generation. *Chem. Mater.* **21**, 3763–3772 (2009).
55. Ponomarev, E. A. & Peter, L. M. A comparison of intensity-modulated photocurrent spectroscopy and photoelectrochemical impedance spectroscopy in a study of photoelectrochemical hydrogen evolution at p-Inp. *J. Electroanal. Chem.* **397**, 45–52 (1995).

Acknowledgements

We especially thank A3 Foresight Program giving an opportunity to research under the cooperation of J.S.L.'s (Korea) and K.D.'s (Japan) groups. This work was supported by Korean Centre for Artificial Photosynthesis (NRF-2011-C1AAA0001-2011-0030278), and Basic Science Research Program (2012-017247) funded by the Ministry of Science, ICT and Future Planning of Republic of Korea.

Author contributions

J.S.L., K.D. and J.K. planned the project. J.Y.K. managed and performed all the detailed experiments, and J.-W.J. helped her in material synthesis. G.M. and D.H.Y. designed the closed circulation system and electrochemical setup, respectively. All the authors discussed the results and commented on the manuscript.

Additional information

Supplementary information accompanies this paper at http://www.nature.com/scientificreports

Competing financial interests: The authors declare no competing financial interests.

How to cite this article: Kim, J.Y. *et al.* Single-crystalline, wormlike hematite photoanodes for efficient solar water splitting. *Sci. Rep.* **3**, 2681; DOI:10.1038/srep02681 (2013).